

PCCP

Accepted Manuscript



This is an *Accepted Manuscript*, which has been through the Royal Society of Chemistry peer review process and has been accepted for publication.

Accepted Manuscripts are published online shortly after acceptance, before technical editing, formatting and proof reading. Using this free service, authors can make their results available to the community, in citable form, before we publish the edited article. We will replace this *Accepted Manuscript* with the edited and formatted *Advance Article* as soon as it is available.

You can find more information about *Accepted Manuscripts* in the [Information for Authors](#).

Please note that technical editing may introduce minor changes to the text and/or graphics, which may alter content. The journal's standard [Terms & Conditions](#) and the [Ethical guidelines](#) still apply. In no event shall the Royal Society of Chemistry be held responsible for any errors or omissions in this *Accepted Manuscript* or any consequences arising from the use of any information it contains.

Physical Chemistry Chemical Physics

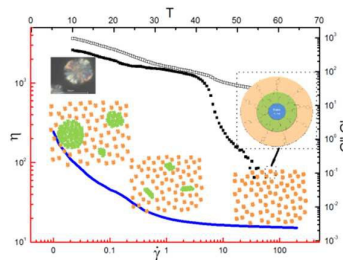
ARTICLE

Received 00th January 20xx,
 Accepted 00th January 20xx
 DOI: 10.1039/x0xx00000x
 www.rsc.org/

Comparison Studies of Rheological and Thermal Behaviors of Ionic Liquid and Nanoparticle Ionic Liquid

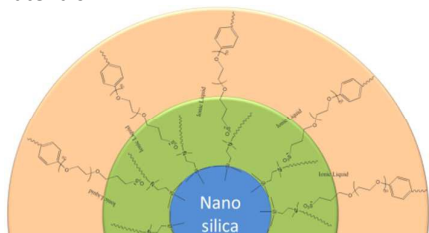
Yiting Xu, Qiang Zheng, Yihu Song*

Novel nanoparticle ionic liquids (NIL) is prepared by grafting modified nanoparticles with long-chain ionic liquid (IL). The NIL behaves like liquid at ambient temperature. We study the rheological behavior of IL and NIL over the range of 10–55 °C and find an extraordinary difference of IL and NIL: a small content of nanosilica (7 %) moderately improves crystallinity by 7 % of poly(ethylene glycol) (PEG) segment in IL, and it improves dynamic moduli significantly (by 5 times at room temperature). It retards the decay temperature (by 10 °C) of dynamic moduli during heating as well. The thermal rheological hysteresis observed during heating-cooling temperature sweeps is ascribed to the melting-recrystallization of PEG segments. Meanwhile, the IL and NIL express accelerated crystallization behavior in comparison with the oligomeric anion. For the first time, we find that IL and NIL are able to form nanoparticles-contained spherulites at room temperature after a long time aging.



1. Introduction

Nanoparticles have been extensively used as fillers to improve physical or chemical properties of polymers. Nanoparticles are commonly functionalized by grafting polymer chains on the surface in order to improve their dispersity^{1,2}. A series of nanoparticles behaving like solvent-free liquids at ambient temperature could be produced by adjusting the size of nanocore and molecular structure of grafting components³. Their properties (such as thermal and magnetic conductances and photoluminescence) could be conveniently tailored by constructing the nanostructured cores using oxides³⁻⁶, carbon⁷⁻¹¹, metals¹²⁻¹⁴, or biomaterials^{4,15}, which may lead to many potential applications in, for example, magnetic fluids and luminescent materials^{5,16,17} as well as lubricants with simultaneous reinforcement and plasticization effects to polymer materials¹⁸.



Scheme 1. Illustration of structure for NIL with a nanosilica core. The covalently attached corona has terminal ammonium functionality and the canopy consists of a low molecular weight, sulfate-terminated PEG covalently connected to a nonylphenyl tail

Two kinds of liquid-like nanoparticle materials have been achieved. The first is synthesized by attaching flexible silicone chains onto nanoparticle surface⁸ and the second is prepared by decorating nanocore with a covalently attached corona bearing ionic terminal functional groups, followed by replacing the small counterion by an oligomeric one¹⁹, for example, replacing Cl⁻ by C₉H₁₉-C₆H₄-(OCH₂CH₂)₂₀O(CH₂)₃-SO₃⁻, to form a canopy layer²⁰. The later with an organic shell of at least 60 % in content²¹ (Scheme 1) is referred as nanoparticle ionic liquid (NIL). The organic shell itself constituted of an ionized oligomer is usually a kind of non-volatile, non-flammable and thermally stable ionic liquid (IL) at ambient temperature²². The IL may exhibit complicated thermal behaviors like supercooling, glassy formation and solid-solid phase transition over a wide temperature range²³, which is, to a large extent, associated with the strong ionic interactions^{24,25}.

The tethered oligomers in the canopy layer of NIL behave as incompressible fluid^{1,26-29} and provide lubrication effect for dispersion and movement of the nanocores. Through adjusting the core size and grafting density, the produced NILs all behave in a liquid-like manner at relatively high temperatures. The migration of oligomeric counterions between different nanocores^{29,30} is shown to influence conductivity, glass transition temperature (T_g), local dynamics and rheology of NIL³¹. On the other hand, both IL and NIL may undergo complicated crystallization under specific conditions, which is of importance for storage and application of NIL materials. However, the rheological and crystallization behaviors of both IL and NIL at low temperatures are not yet investigated up to date.

MOE Key Laboratory of Macromolecular Synthesis and Functionalization, Department of Polymer Science and Engineering, Zhejiang University, Zheda Road No. 38, Hangzhou 310027, China. E-mail address: s_yh0411@zju.edu.cn (Y. Song);

ARTICLE

Physical Chemistry Chemical Physics

Herein we synthesis IL and NIL by ion exchange reaction of dimethyloctadecyl-[3-(trimethoxysilyl)propyl]ammonium chloride $[(\text{CH}_3\text{O})_3\text{Si}(\text{CH}_2)_3\text{N}^+(\text{CH}_3)_2(\text{C}_{18}\text{H}_{37})\text{Cl}^-]$, either free or grafted on nanosilica, with surfactant nonylphenyl poly(ethylene glycol) ether potassium sulfate [NPEP, $\text{C}_9\text{H}_{19}-\text{C}_6\text{H}_4-(\text{OCH}_2\text{CH}_2)_{20}-\text{O}(\text{CH}_2)_3-\text{SO}_3^-\text{K}^+$]. According to differential scanning calorimetry (DSC) test, both IL and NIL exhibit complicated thermal behaviors with multi-peaks of melting and crystallization. We studied their rheological behaviors over the temperature range of 10–55 °C and found both IL and NIL exhibit thermal rheological hysteresis during heating-cooling cycles at 1 °C/min, which could be ascribed to the melting-recrystallization behavior. When the heating and cooling rates were 0.1 °C/min, the hysteresis of IL disappeared while it still exist in NIL. The modulus and transition temperature of NIL are significantly influenced by nanocore. For the first time, IL and NIL are found to crystallize to spherulites (40–75 μm diameter) after a long time aging at ambient temperature according to polarizing microscope (POM) observation. Investigation of the complicated thermal and rheological behaviors of NIL could provide guidance to its storage and application.

2. Experimental

2.1. Material

Nanosilica (Ludox AS-30, 30 wt% dispersion in water, 12 nm diameter) and nonylphenyl poly(ethylene glycol) ether potassium sulfate [NPEP, $\text{C}_9\text{H}_{19}-\text{C}_6\text{H}_4-(\text{OCH}_2\text{CH}_2)_{20}-\text{O}(\text{CH}_2)_3-\text{SO}_3^-\text{K}^+$] were received from Sigma-Aldrich Chem. Co., USA. Dimethyloctadecyl-[3-(trimethoxysilyl)propyl]ammonium chloride $[(\text{CH}_3\text{O})_3\text{Si}(\text{CH}_2)_3\text{N}^+(\text{CH}_3)_2(\text{C}_{18}\text{H}_{37})\text{Cl}^-]$, DC 5700, also named as AEM 5700, 42% methanol solution] was a product from Dow Corning Co., USA.

2.2. Preparation of NIL

Briefly, 10 ml of nanosilica dispersion was diluted by 20 ml ultrapure water (18.25 μs/cm) and then 10 g DC 5700 solution was added in. The precipitate aged for 24 h at ambient temperature was rinsed with water and methanol. The dried solid was dissolved in ethanol and centrifuged at 10,000 rpm for 20 min to remove insoluble particles. The supernatant was collected and evaporated to leave behind silica chloride nanosalt. The NIL was prepared by treating 1 g silica chloride nanosalt with 1.5 g NPEP in 50 ml chloroform for 5 h at ambient temperature. The solution was extracted with 20 ml ultrapure water for three times. The dispersion was evaporated at 65 °C, dispersed in 20 ml acetone, centrifuged, and then dried at 65 °C. Finally, the NIL was dispersed in water and was dialyzed in Snake Skin dialysis tubing (3500 MWCO, Pierce) using deionized water until ion conductance was below 2 μs/cm. The product was obtained after drying the dispersion. The prepared NIL contains 56.39% C, 9.47 % H and 0.68 % N according to element analysis.

2.3. Preparation of IL

2 | Physical chemistry chemical physics, 2015, 00, 1-3

The IL was prepared by treating 1 g DC 5700 solution with 1.5 g NPEP in 50 ml chloroform for 5 h at ambient temperature. The solution was exacted with 20 ml ultrapure water for three times. The IL was obtained after drying the dispersion. The prepared IL contains 58.25% C, 9.56 % H and 0.62 % N according to element analysis.

2.4. Measurement

Organic contents of IL and NIL were determined by TGA measurement on a thermogravimetric analyzer (Q50, TA Instruments, USA) using high purity nitrogen as balance gas and sample gas at flow velocities of 40 ml/min and 60 ml/min, respectively. Elementary composition of urea l-tartaric acid was determined by an elemental analyzer (Carlo Erba EA1110, German). Differential scanning calorimetry (DSC) measurements were performed using a differential scanning calorimeter (Q100, TA, USA) at cooled and heated rates of 5 °C/min under high purity nitrogen purge gas of 50 ml/min. The samples were heated to a prescribed temperature to eliminate thermal history and thermal flows during the cooling and the second heating runs were recorded. Bright-field transmission electron microscopy (TEM) images were taken at an accelerate voltage of 120 kV using an electron microscope (Jeol JEM-1200EX, Nippon Electric Co. Ltd., Japan). The samples were prepared by placing a few drops of IL and NIL dispersed in ethanol (2% wt/vol) on a copper grid, and evaporating the solvent. Rheology measurements were conducted on a rheometer (AR G2, TA, USA) using a plate-and-plate geometry (20 mm in diameter, 500 μm in gap). Steady rheology was performed at strain rate from 0.01 s⁻¹ and 200 s⁻¹ and temperature-sweep dynamic rheology was performed at 6.28 rad/s frequency and 1 % strain amplitude. POM observations were carried out by using an optical microscope (BX51, Olympus) equipped with an Olympus camera and a temperature-controlled hot stage (THMS600, Linkam Sci. Instrument Ltd., UK). The specimens were sandwiched between two microscope cover slips for observation. X-ray diffraction (XRD) was performed using a X-ray diffractometer (Rigaku Ultima IV X, Japan) using CuKα radiation (λ=1.54 Å).

3. Results and discussion

3.1. Crystallization and melting behaviors

The ion exchange reaction of $(\text{CH}_3\text{O})_3\text{Si}(\text{CH}_2)_3\text{N}^+(\text{CH}_3)_2(\text{C}_{10}\text{H}_{21})_2\text{Cl}^-$ with NPEP yields IL (free of nanosilica) and NIL (anchored on nanosilica). Both IL and NIL express excellent fluidity (insets in Figure 1a and Figure 1b). The IL appears as an amorphous liquid (Figure 1a) while NIL contains monodispersed particles of 15 nm in diameter (Figure 1b) simply calculated from the TEM image. The nanocores in NIL remain intact, showing that the IL layer is grafted to the surface of nanosilica⁴. TGA in nitrogen atmosphere shows that NIL and IL contain no solvent, and their decomposition temperatures are above 200 °C (insets in Figure 1a). The NIL contains around 7 wt.% of silica according to its weight residue

at 600 °C. According to element analysis, IL and NIL contain 57 wt.% and 54 wt.% of poly(ethylene glycol) (PEG) segment, respectively.

The thermal behaviors of IL and NIL were tested by DSC. In Figure 2a, NPEP exhibits a very tiny crystallization peak at -19.0 °C during cooling and a remarkable cold crystallization peak (T_{cc}) at -18.5 °C. Two melting temperatures (T_m) appeared at 15.0 °C (strong) and 31.0 °C (weak) during heating. In comparison, Bourlinos *et al.*⁴ observed $T_g = -55$ °C, $T_{cc} = -10$ °C and $T_m = 15$ °C for NPEP during cooling and heating at rates of 10 °C/min. As shown in Figure 2a, IL exhibits three crystallization temperatures (T_c) at 7.2 °C (weak), -6.8 °C (weak) and -30.1 °C (strong) during cooling and one melting peak (T_m) at 12.5 °C during heating. Being different from Bourlinos *et al.*⁴ who observed a rather simple thermal behavior with $T_{cc} = -20$ °C and $T_m = 32$ °C for nanoanatase-based NIL, we detected three crystallization peaks (T_c) (14.5 °C, very weak; -4.6 °C, very weak; and -32.7 °C, strong) and two melting temperatures (T_m) (11.9 °C, strong; and 30.0 °C, very weak) in our NIL. The appearance of cold crystallization in NPEP is ascribed to the low ability to form nuclei as well as low chain mobility. On the other hand, the IL and NIL exhibit strong crystallization peak during cooling while the cold crystallization during heating is absent, revealing an accelerated nuclei formation ability in comparison with NPEP. The percent of crystallinities of PEG segment in NPEP, IL and NIL are determined according to $\Delta H_m/\Delta H_m^0$ ³², as shown in Table 1. Here, ΔH_m is melting enthalpy of the main melting peak and $\Delta H_m^0 = 188.9$ J/g³³ represents melting enthalpy of perfect PEG crystal. Crystallinities of PEG segments in IL and NIL are much higher than those in NPEP, suggesting that the crystallization capability of PEG segments is largely improved after ion-exchange reaction. The nanoanatase-based NIL exhibits lower crystallization extent than NPEP possibly because nanoanatase prevents the molecular rearrangement for crystal formation²⁶. However, the PEG segments in the IL and NIL are easy to crystallize in comparison with pure NPEP. It is originated from the large silica size and weak anion aggregation³¹.

Nonisothermal crystallizations of IL and NIL are highly dependent on thermal history. The data are presented in Figure 2b. There are very small exothermic peak at 9.6 °C and 18.9 °C, respectively, being similar to the highest T_c with small enthalpies listed in Table 1. The crystals of IL and NIL display tiny and broad melting peaks, up to 25 °C and 35 °C, respectively. Their low crystallinity degree reflecting a slow partial melting-recrystallization mechanism³⁴. Note that at

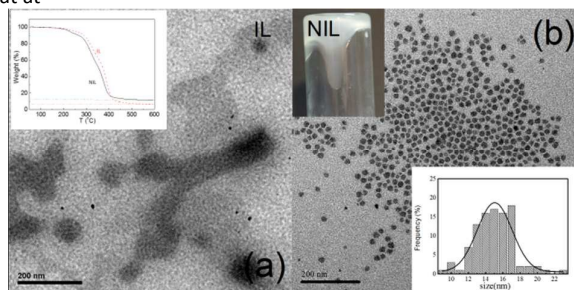


Figure 1. TEM micrographs of IL (a) and NIL (b). The insets in (a) show photo of IL and TG traces of IL and NIL and the insets in (b) show photo of NIL and its size distribution.

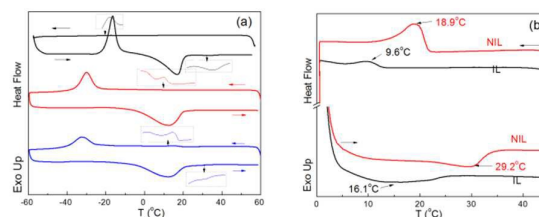


Figure 2. DSC cooling and successive heating traces of NPEP, IL and NIL: (a) temperature range: from 60 °C to -60 °C; (b) from 50 °C to 0 °C, respectively. Cooling and heating rates: 5 °C/min. The thin curves in (a) display enlarged plots of the regional thermal transitions.

Table 1 Melting, crystallization temperatures, enthalpies and crystallinities (PEG segments) for NPEP, IL and NIL.

Sample	T_c (°C)	ΔH_c (J/g)	T_m (°C)	ΔH_m (J/g)	Crystallinity (%)
NPEP	-20.0	0.81	15.0 ^b	49.43	37.3
	-18.5 ^{a,b}	41.76	31.5	0.60	
IL	7.5	0.22	12.5 ^b	55.35	51.4
	-8.0	0.13	-	-	
	-30.1 ^b	27.8	-	-	
NIL	15.2	0.80	11.9 ^b	59.0	58.9
	-4.4	0.01	32.9	0.14	
	-32.7 ^b	25.30	-	-	

^a cold crystallization; ^b main thermal transition peaks.

temperatures (T) above 0 °C, NIL exhibits a higher crystallization capacity than IL. Such peculiar behavior is not observed in NPEP at $T > 0$ °C, confirming that the weak anion aggregation and the nanosilica accelerate the PEG crystallization process. Although the process is very slow, the crystals formed at ambient temperature still form microscale spherulites after a long-term aging (see Figure 3).

POM observations show sparse spherulites of about 40 μm and 75 μm (maximum diameter) in IL and NIL, respectively (insets in Figure 3). The samples were obtained after being aged in a glass spawn bottle for days at ambient temperature (below 15 °C). Because NPEP does not form spherulites under the same condition, the formation of spherulites in IL and NIL is attributed to regular arrangement of the zwitterion molecules resulted from ion-exchange reaction. When the samples were heated to about 25 °C, the spherulites start to melt. It is hard to *in-situ* observe the spherulite growth in the very slow process (more than three days). It is also hard to observe the spherulites using TEM and scanning electron microscopy because the high electrical beam irradiated on the samples can easily melt the spherulites. According to XRD pattern (Figure 3), NIL exhibits characteristic diffraction peaks at 19.1 ° and 23.3 ° according to the (120) and (032) planes of PEG segment³⁵ in NPEP. The XRD pattern of IL exhibits an amorphous peak due its T_m below the testing temperature.

3.2 Rheological behaviors

The T -sweep dynamic rheology and steady rheology at different temperatures are shown in Figures 4a and 4b, respectively, for IL. The sample was first heated to 50 °C to remove thermal history and was then cooled to 10 °C and kept for 30 min before testing. Through the whole T range from 10

ARTICLE

Physical Chemistry Chemical Physics

°C to 55 °C, loss modulus G'' of IL is higher than storage modulus G' (Figure 4a), revealing a liquid-like behavior. During heating, G' increases from 50 Pa to 58 Pa with increasing T from 20 °C to 25 °C and then reduces rapidly by more than two orders of magnitude, becoming undetectable at $T > 40$ °C. On the other hand, G'' in general decreases with increasing T but exhibits a small accelerated drop from 35 °C to 40 °C. In the cooling run, the G'' curve coincides with the heating one but exhibits a slight hysteresis at $T < 40$ °C. G' shows an abrupt increase at around 25 °C with decreasing T and exceeds its original value at 10 °C by about 17 %. The marked variations of G' during a heating-cooling run could be readily related to the melting and crystallization behaviors of PEG segments in IL. The crystals form during isothermal treatment before test at 10 °C undergo melting during heating and IL would recrystallize during cooling, which causes the marked rheological hysteresis. According to steady flow curves of viscosity (η) as a function of shear rate ($\dot{\gamma}$) (Figure 4b), IL exhibits a marked shear thinning at $T < 35$ °C and turns to Newtonian fluid at $T > 40$ °C. The T range for the transition from shear thinning to Newtonian fluids is in agreement with the significant G' drop in the T -sweep (Figure 4a). The activation energy of flow at the large $\dot{\gamma}$ limit is determined as 45.7 kJ/mol (inset in Figure 4b). The steady rheology measurements are repeatable as exemplarily demonstrated from two successive cycles by increasing and decreasing $\dot{\gamma}$ at 25 °C, proving that the structure is free of chemically debonding²⁷. The shear-thinning behavior might be related to the randomization of zwitterion facilitated by accelerated ion-exchange reaction and the behavior is magnified by the crystals inside. Further investigation the T -sweep within a narrow T range (35–40 °C) at a slow rate of 0.1 °C/min reveals reversible rheology related to the melting-recrystallization in the very slow heating-cooling run.

NIL also demonstrates a liquid-like behavior at 10 - 55 °C (Figure 4c). Because the nanocore weakens the mobility of attached zwitterion molecules and increases the crystallinity of PEG segments, NIL exhibits moduli about 5 times higher than IL at 10 °C. Being different from Bourlinos *et al.*⁴ who reported a normal viscosity decrease during heating anatase-based NIL from 40 °C to 80 °C, we observed a complicated T -dependent rheology in our NIL. When NIL being heated to above 40 °C, G' exhibits a rapid decay by more than three orders of magnitude. Besides, a remarkable increment appears during cooling from 50 °C to 29 °C, exhibiting a significant hysteresis. The hysteresis can also be observed from the heating and cooling G'' curves, which do not coincide at $T < 45$ °C. The T -sweeps at 0.1 °C/min in a narrow range of 35–45 °C also reveals the G' hysteresis (inset in Figure 4c). When NIL was pretreated at 35 °C for 30 min before testing, it shows a gel-like behavior ($G' \approx G''$) while this gel-like behavior cannot recover upon cooling. Furthermore, the hysteresis of NIL is more remarkable than IL, and the G' variation of NIL is slower than that of IL, suggesting that the nanocore retards the structural variation in combination with the melting-recrystallization of IL. According to steady rheology curves (Figure 4d), NIL exhibits shear thinning at $T \leq 40$ °C. Being similar with other nanofluids^{36–38}, η mainly decreases at $\dot{\gamma} < 1$ s⁻¹ and NIL

behaves as Newtonian fluid at high rates. However, the Newtonian behavior of NIL (at $T \geq 45$ °C) demonstrates that the shear-thinning is related to the temperature-dependent structure^{19, 20}. The activation energy of NIL flow (inset in Figure 4d) at large $\dot{\gamma}$ limit is the same as IL. In conclusion, NIL and IL share the same microscale structure transition during heating-cooling process.

Both IL and NIL crystallize at ambient temperature. They form spherulites after a rather long time (Figure 3), and experience crystallization in the T ranges of 6–13 °C and 10–22 °C, respectively (Figure 2b). Once the crystallites form in IL and NIL at $T > 0$ °C, they exhibit a broad melting range up to 25 °C and 35 °C, respectively (Figure 2b). The slight G' increment of IL with increasing T from 20 °C

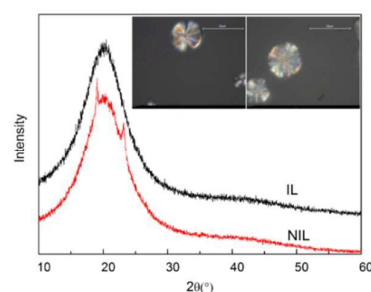


Figure 3. XRD curves of IL and NIL crystallized at room temperature. The insets in (a) and (b) are photos of IL and NIL. The insets show POM photographs of the spherulites formed in IL (left) and NIL (right) at ambient temperature.

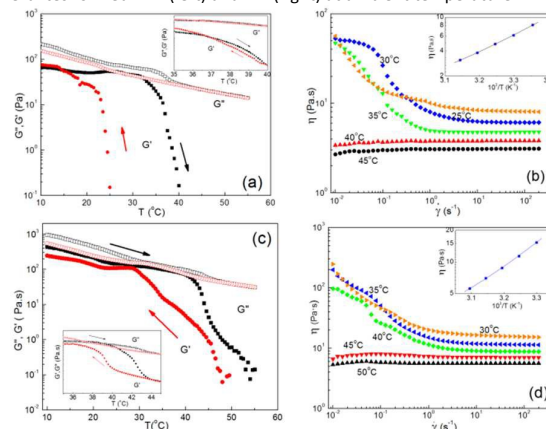


Figure 4. T -sweep dynamic rheology during a heating-cooling run at 1 °C/min (a and c) and steady rheology (b and d) for IL (a and b) and NIL (c and d). The insets in (a) and (c) show the T -sweep at 0.1 °C/min and those in (b) and (d) shows η at $\dot{\gamma} = 10^2$ s⁻¹ as a function of reciprocal temperature.

to 25 °C (Figure 4a) as well as the G' plateau of NIL at 23–32 °C in the broad range T -sweep and the gel-like behavior in the narrow range T -sweep (Figure 4c) are ascribed to the melting-recrystallization during heating. Flow fields may destroy interconnects between crystallites³⁴, leading to thinning flow at low temperatures. At high rates, both IL and NIL exhibit a steady flow following Arrhenius law as a function of T .

4. Conclusions

Both IL and NIL exhibit particular temperature-dependent rheological behaviors with a hysteresis loop during heating-cooling cycles. It is related to the melting-recrystallization behavior of the PEG segments. Low crystallization degree endows IL and NIL with shear thinning behavior at low temperatures. On the other hand, destruction of crystals by heating make them behave as Newtonian fluid. The ion-exchange reaction and the nanocores as nuclei accelerate the crystallization process of PEG segments. Both IL and NIL crystallize slowly at ambient temperature, and form spherulites in micron scale.

Acknowledgements

This work is supported by National Natural Science Foundation of China (51373149 and 51333004), National Natural Science Foundation of Zhejiang Province (R14E030003), and Key Technology Program of Guizhou Province (2013-6016).

Notes and references

- P. Akcora, H. Liu, S. K. Kumar, J. Moll, Y. Li, B. C. Benicewicz, L. S. Schadler, D. Acehan, A. Z. Panagiotopoulos, V. Pryamitsyn, V. Ganesan, J. Ilavsky, P. Thiyagarajan, R. H. Colby and J. F. Douglas, *Nat. Mater.*, 2009, 8, 354-359.
- Y. Jiao and P. Akcora, *Macromolecules*, 2012, 45, 3463-3470.
- A. B. Bourlinos, R. Herrera, N. Chalkias, D. D. Jiang, Q. Zhang, L. A. Archer and E. P. Giannelis, *Adv. Mater.*, 2005, 17, 235-237.
- A. B. Bourlinos, S. R. Chowdhury, R. Herrera, D. D. Jiang, Q. Zhang, L. A. Archer and E. P. Giannelis, *Adv. Funct. Mater.*, 2005, 15, 1285-1290.
- D. P. Liu, G. D. Li, Y. Su and J. S. Chen, *Angew. Chem. Int. Edit.*, 2006, 45, 7370-7373.
- A. B. Bourlinos, A. Stassinopoulos, D. Anglos, R. Herrera, S. H. Anastasiadis, D. Petridis and E. P. Giannelis, *Small*, 2006, 2, 513-516.
- Y. A. Lei, C. X. Xiong, H. Guo, J. L. Yao, L. J. Dong and X. H. Su, *J. Am. Chem. Soc.*, 2008, 130, 3256-3257.
- A. B. Bourlinos, V. Georgakilas, N. Boukos, P. Dallas, C. Trapalis and E. P. Giannelis, *Carbon*, 2007, 45, 1583-1585.
- Q. Li, L. J. Dong, Y. Liu, H. A. Xie and C. X. Xiong, *Carbon*, 2011, 49, 1047-1051.
- L. S. Wu, B. Q. Zhang, H. Lu and C. Y. Liu, *J. Mater. Chem. A.*, 2014, 2, 1409-1417.
- P. P. Li, Y. P. Zheng, Y. W. Wu, P. Qu, R. L. Yang and A. B. Zhang, *Appl. Surf. Sci.*, 2014, 314, 983-990.
- S. C. Warren, M. J. Banholzer, L. S. Slaughter, E. P. Giannelis, F. J. DiSalvo and U. B. Wiesner, *J. Am. Chem. Soc.*, 2006, 128, 12074-12075.
- D. Batra, S. Seifert, L. M. Varela, A. C. Y. Liu and M. A. Firestone, *Adv. Funct. Mater.*, 2007, 17, 1279-1287.
- Y. P. Zheng, J. X. Zhang, L. Lan, P. Y. Yu, R. Rodriguez, R. Herrera, D. Y. Wang and E. P. Giannelis, *Chemphyschem*, 2010, 11, 61-64.
- A. W. Perriman, H. Colfen, R. W. Hughes, C. L. Barrie and S. Mann, *Angew. Chem. Int. Edit.*, 2009, 48, 6242-6246.
- K. Y. A. Lin and A. H. A. Park, *Environ. Sci. Technol.*, 2011, 45, 6633-6639.
- Y. Park, J. Decatur, K. Y. A. Lin and A. H. A. Park, *Phys. Chem. Chem. Phys.*, 2011, 13, 18115-18122.
- Q. Li, L. J. Dong, L. B. Li, X. H. Su, H. A. Xie and C. X. Xiong, *Carbon*, 2012, 50, 2056-2060.
- R. Rodriguez, R. Herrera, L. A. Archer and E. P. Giannelis, *Adv. Mater.*, 2008, 20, 4353-4358.
- R. Rodriguez, R. Herrera, A. B. Bourlinos, R. Li, A. Amassian, L. A. Archer and E. P. Giannelis, *Appl. Organomet. Chem.*, 2010, 24, 581-589.
- A. B. Bourlinos, S. R. Chowdhury, D. D. Jiang and Q. Zhang, *J. Mater. Sci.*, 2005, 40, 5095-5097.
- A. Koenig, M. Stepanski, A. Kuzlik, P. Keil and C. Weller, *Chemical Engineering Research & Design*, 2008, 86, 775-780.
- P. M. Dean, J. M. Pringle and D. R. MacFarlane, *Phys. Chem. Chem. Phys.*, 2010, 12, 9144-9153.
- K. Fumino, T. Peppel, M. Geppert-Rybczynska, D. H. Zaitsau, J. K. Lehmann, S. P. Verevkin, M. Kockerling and R. Ludwig, *Phys. Chem. Chem. Phys.*, 2011, 13, 14064-14075.
- R. K. Blundell and P. Licence, *Phys. Chem. Chem. Phys.*, 2014, 16, 15278-15288.
- A. Chremos, A. Z. Panagiotopoulos and D. L. Koch, *J. Chem. Phys.*, 2012, 136.
- A. Chremos and A. Z. Panagiotopoulos, *Phys. Rev. Lett.*, 2011, 107.
- A. Chremos, A. Z. Panagiotopoulos, H.-Y. Yu and D. L. Koch, *J. Chem. Phys.*, 2011, 135.
- B. Hong and A. Z. Panagiotopoulos, *Soft Matter*, 2013, 9, 6091-6102.
- M. L. Jespersen, P. A. Mirau, E. von Meerwall, R. A. Vaia, R. Rodriguez and E. P. Giannelis, *Acs Nano*, 2010, 4, 3735-3742.
- A. B. Bourlinos, E. P. Giannelis, Q. Zhang, L. A. Archer, G. Floudas and G. Fytas, *Eur. Phys. J. E.*, 2006, 20, 109-117.
- K. Y. Mya, K. P. Pramoda and C. B. He, *Polymer*, 2006, 47, 5035-5043.
- S. Hong, L. Z. Yang, W. J. MacKnight and S. P. Gido, *Macromolecules*, 2001, 34, 7009-7016.
- V. S. Papkov, M. I. Buzin, M. V. Gerasimov and E. S. Obolonkova, *Macromolecules*, 2002, 35, 1079-1090.
- X. Hu, J. Z. Xu, G. J. Zhong, X. L. Luo and Z. M. Li, *J. Polym. Res.*, 2011, 18, 675-680.
- A. Mariano, M. Jose Pastoriza-Gallego, L. Lugo, A. Camacho, S. Canzonieri and M. M. Pineiro, *Fluid Phase Equilib.*, 2013, 337, 119-124.
- B. Aladag, S. Halelfadl, N. Doner, T. Mare, S. Duret and P. Estelle, *Appl. Energy*, 2012, 97, 876-880.
- M. Jose Pastoriza-Gallego, L. Lugo, J. Luis Legido and M. M. Pineiro, *Nanoscale Res. Lett.*, 2011, 6.